THE ASTROPHYSICAL JOURNAL, 384:197–211, 1992 January 1

AN INFRARED STUDY OF THREE WOLF-RAYET RING NEBULAE

J. S. MATHIS,[1] J. P. CASSINELLI,[1] K. A. VAN DER HUCHT,[2] T. PRUSTI,[3] P. R. WESSELIUS,[3] AND P. M. WILLIAMS[4]
Received 1991 May 2; accepted 1991 July 5

ABSTRACT

We have studied the *IRAS* colors of the ring nebula RCW 58 surrounding the Wolf-Rayet star HD 96548 (= WR 40; type WN 8) by analyzing the *IRAS* survey data with the Groningen Exportable High-Resolution Analysis system (GEISHA) and by using the Chopped Photometric Channel high-resolution imaging at 50 μm. Additional *JHKLM* photometry of the exciting star of RCW 58, and also of HD 50896 (WR 6, type WN 5), exciting the bubble S308, and of HD 192163 (WR 136, type WN 6), exciting the bubble nebula NGC 6888, have been obtained.

We have estimated the emission from dust in all three bubbles by subtracting the stellar contributions to the *IRAS* images and correcting the *IRAS* fluxes for atomic emissions. Except for the 12 μm filter, the atomic contributions do not comprise the bulk of the observed fluxes. As compared to the interstellar medium (ISM) and clouds, the dust emissions are very weak in 12 μm relative to 25 μm but have $F(60)/F(100) > 1$, compared to ≤ 0.2 for the ISM, showing that the grains are heated by the enhanced radiation field in the vicinity of the central star.

The dust emission is analyzed by means of several models. For RCW 58, the diffuse dust model of Mathis, Rumpl, & Nordsieck, with optical constants as modified by Draine & Lee and grains in the size range 0.005–0.25 μm, produces fairly good agreement with the observations, except that the required radiation field is higher (≈ 100 eV cm^{-3}) than one would expect from the mean distance of the bubble from the star (≈ 44 eV cm^{-3}) with the stellar temperature we adopt. It is possible to fit the spectrum with the expected radiation field if a combination of small grains (0.002 μm–0.008 μm) are in the inner part of the nebula and somewhat larger ones (0.005 μm–0.05 μm) farther out. For S308 and NGC 6888, if there is enough radiation to produce the proper $F(25)/F(60)$ from MRN grains the $F(60)/F(100)$ flux ratio is too large. However, small grains transiently heated by random absorptions of stellar photons produce too large a $F(60)/F(100)$ ratio at the observed $F(25)/F(60)$. For these objects we find fits to both *IRAS* ratios by assuming that there are small grains transiently heated in the inner parts of the bubbles and standard interstellar grains in the outer portions. The masses of material in the nebulae are consistent with most of the matter being stellar for RCW 58 and a substantial amount of material being contributed by the swept-up ISM for S308 and NGC 6888. However, the masses are very sensitive to both the photometry and to the assumptions of the nature of the small grains near the star. Quantitative estimates of the mass are only order of magnitude.

Graphs are given which allow an easy estimation of the nebular mass for other situations for nebular excitation. The principal parameter is the dilution factor of the stellar radiation.

Subject headings: dust, extinction — ISM: individual (RCW 58, S308, NGC 6888) — radiation mechanisms: thermal — stars: Wolf-Rayet

1. INTRODUCTION

The spectacular ring nebula RCW 58 around the WN 8 star HD 96548 (= WR 40; van der Hucht et al. 1988) has been observed by the *IRAS* survey instrument and by the *IRAS* Chopped Photometric Channel (CPC). In Hα, RCW 58 is extended and fairly symmetrical, with outer angular dimensions of about $7' \times 9'$. Morphological studies by Chu (1982), Chu, Treffers, & Kwitter (1983), and Smith et al. (1988) show that in Hα and [N II] the nebula has both a clumpy and a filamentary structure, with the clumps having sharp inner and diffuse outer edges. In [O III] the nebula is more extended, diffuse, and without clumps. Chu (1982) first suggested that the [O III] ring represents a wind-blown bubble, enveloping clumpy stellar ejecta visible in Hα and [N II]. An overall review of WR nebulae has been given by Chu (1991).

One would like to determine the masses of stellar ejecta and also the swept-up interstellar matter. Because of the clumpy appearance of the nebula, Chu (1982) concluded that at least part of the mass of the nebula originates from an event of bulk ejection at some phase in the evolution of the central star. Smith et al. (1988) suggested that the ejection occurred during a red-supergiant phase of the central star because, among other reasons, of the presence of dust in the nebula evidenced by the *IRAS*-CPC 50 μm image shown by van der Hucht et al. (1985). In this paper we will investigate the extent to which the *IRAS* data of RCW 58 can be attributed to line emission, and then estimate the dust properties and mass of the nebula.

From *IRAS* survey data images, Van Buren & McCray (1988, hereafter VBM88) concluded that dust is present in the ring nebula S308 around HD 50896 (= EZ CMa = WR 6, type WN 5), but suggested that the *IRAS* image of NGC 6888 around HD 192163 (= WR 136, type WN 6) is mainly caused by line emission. Marston & Meaburn (1988, hereafter MM88) suggested that the *IRAS* image of NGC 6888 is mainly due to

[1] Astronomy Department, University of Wisconsin-Madison, 475 N. Charter Street, Madison, WI 53706-1582.
[2] SRON Space Research Utrecht, Sorbonnelaan 2, 3584 CA Utrecht, The Netherlands.
[3] SRON Space Research Groningen, P.O. Box 800, 9700 AV Groningen, The Netherlands.
[4] Royal Observatory, Blackford Hill, Edinburgh, EH9 SHJ, Scotland, UK.

TABLE 1A

ADOPTED STELLAR PARAMETERS FOR THE WOLF-RAYET STARS EXCITING THE NEBULAE

Parameter	RCW 58	S308	NGC 6888
Star name	HD 96548 = WR 40	HD 50896 = WR 6	HD 192163 = WR 136
Type	WN 8	WN 5	WN 6
v (line free) (mag)	7.7 (1)	7.3 (1)	7.64 (3)
$(b-v)$ (line free) (mag)	0.18 (1)	−0.03 (1)	0.33 (3)
$(b-v)_0$ (mag)	−0.28 (1)	−0.23 (6)	−0.30 (6)
A_V (mag)	1.89 (1)	0.82 (6)	2.01 (6)
A_V (line free) (mag)	1.73 (1)	0.75 (6)	1.84 (6)
M_V	−5.8 (1)	−4.8 (6)	−5.7[a]
Distance (kpc)	2.1[b]	1.80[b]	1.82[a]
T_* (K)	32000 (2)	57500 (4)	50000 (7)
$\log(L/L_\odot)$	5.50 (2)	5.30 (4)	5.50 (7)
$R_*/R_\odot$	18 (2)	4.7 (4)	7 (7)
Bolometric Correction[c] (mag)	−3.2	−3.7	−3.3
v (C IV) (km s^{-1})	1800 (8)	2500 (5)	2400 (8)
$v(r=\infty)$	1260[d]	1700 (4)	1600 (7)
$M_*/M_\odot$	26 (8)	10 (4)	21 (8)
$\dot{M}$ ($M_\odot$ yr^{-1})	6.3×10^{-5} (4)	1×10^{-4} (4)	1.3×10^{-4} (7)

NOTE.—References given in parentheses after entries.

[a] From Cyg OB1.

[b] Quantity derived from photometry.

[c] From L and M_V listed above entry.

[d] Adopting $v(\infty) = 0.7v$(C IV); Williams & Eenens 1989.

REFERENCES.—(1) Torres-Dodgen & Massey 1988. (2) Nussbaumer et al. 1982. (3) Massey 1984. (4) Hamann et al. 1988. (5) Willis et al. 1989. (6) van der Hucht et al. 1988. (7) Schmutz et al. 1989. (8) Willis 1982.

TABLE 1B

ADOPTED NEBULAR PARAMETERS

Parameter	RCW 58	S308	NGC 6888
Angular size (visible)	7′ × 9′ (1, 2)	40′ × 42′ (8)	12′ × 18′ (8)
v (expansion) (km s^{-1})	87–110 (2, 4)	60 (8)	75 (8)
v (system)	−3–0 (2, 4)	...	...
n_e (cm^{-3})	200 (2, 5, 6)	140 (7)	250 (7)
T_e (K)	7500 (6)	12700 (7)	7500 (6)
He/H	0.23 (6, 7)	0.123	0.209
10^6 N/H[a]	262	123	245
10^6 O/H	525	158	347
10^6 Ne/H	35.5	42	17.5
10^6 S/H	9.4	7.9	10.5
10^6 Cl/H	0.14	0.50	0.17
10^6 Ar/H	4.3	1.5	3.6

NOTE.—References given in parentheses after entries.

[a] Abundances are by numbers, from refs. 6 and 7.

REFERENCES.—(1) Chu 1982. (2) Smith et al. 1988. (3) This study. (4) Chu 1988. (5) Kwitter 1984. (6) Rosa 1987. (7) Rosa & Mathis 1991. (8) Chu et al. 1983.

dust rather than atomic emission. Marston (1991, hereafter M91) estimated the masses of three WR nebulae (NGC 2359, RCW 58, and NGC 6888) from the *IRAS* images, including both the survey filter observations and the CPC at 50 μm and at 100 μm. He estimated nebular masses from the ratios of the 50 μm (or 60 μm) to 100 μm intensities, on the basis of grains which are emitting the radiation without temperature fluctuations.

We will consider the 25, 60, and 100 μm emissions from RCW 58, NGC 6888, and also S308. With the additional information provided by the 25/60 μm flux ratio we are forced to consider grains which are fluctuating in temperature. This transient heating affects the grain emissivity at 60 μm substantially.

2. STELLAR AND NEBULAR PARAMETERS

In the various previous studies of RCW 58 different parameters have been adopted. Table 1A and 1B list the stellar and nebular parameters we used in this study, with references. Since no cluster membership is known for galactic WN 8 stars, we adopt the average values of absolute visual magnitude and intrinsic colors for LMC WN 8 stars. This implies a distance of WR 40 (RCW 58) of 2.1 kpc. Stellar temperature and luminosity have been determined from modeling energy distributions and He II lines by Nussbaumer et al. (1982) and Schmutz, Hamann, & Wessolowski (1989), which agree very well with each other. The bolometric correction BC = −3.2 resulting from the adopted L and M_v values is closer to the value −3.1 found for O9.5 I stars by Voels et al. (1989) than the values −4.2 found for WR stars in binaries (van der Hucht et al. 1988) and −4.5 in open clusters and associations (Smith & Maeder 1989). The latter values were derived by comparison with theoretical mass-luminosity relations. The discrepancy may indicate inadequacies in present-day interior models. The listed mass of WR 40 was derived with a formula given by Willis (1982):

$$M = 1.276 \times 10^{-5} L + v_{\rm esc}^2 R/2G ,$$

TABLE 2

GROUND-BASED INFRARED PHOTOMETRY OF WR 40, WR 6, AND WR 136

Star (Nebula)	WR 40 (RCW 58)	WR 6 (S308)	WR 136 (NGC 6888)
$A(V)$ (mag)	1.73	0.75	1.84
J	6.71, 6.56, 6.57, 6.61[a]	6.42[b]	6.20[c]
H	6.45, 6.44, 6.43, 6.45[a]	6.23[b]	6.09,[d] 5.97[c]
K	6.13, 6.12, 6.12, 6.14[a]	5.91[b]	5.73,[d] 5.60[c]
L	5.58, 5.43, 5.5, 5.50[a]	5.31[b]	4.93,[d] 4.91[c]
M	5.21, 4.94, 5.3, 5.8[a]	4.96[b]	...

[a] Entries were obtained at ESO, through a 15″ diaphragm, on 1980 May 2; 1980 May 2; 1990 March 15; and 1990 April 11, respectively.
[b] Entry obtained at ESO on 1988 May 2 through a 15″ diaphragm.
[c] Entries were obtained at UKIRT and 1984 March 12 through a 12″ diaphragm.
[d] Obtained at SAAO on 1988 August 12 through a 20″ aperture.

where all quantities are expressed in cgs units. The parameters for WR 6 (S308) and WR 136 (NGC 6888) are derived in similar ways, as indicated in Tables 1A and 1B.

3. OBSERVATIONS

3.1. *Ground-Based Infrared Photometry*

The *JHKLM* photometry of WR 6, WR 40, and WR 136 listed in Table 2 was obtained at various epochs by the present authors (KAvdH at ESO; PMW at UKIRT). The results compare well with previous observations of Allen, Swings, & Harvey (1972), Hackwell, Gehrz, & Smith (1974), Cohen, Barlow, & Kuhi (1975), Williams & Antonopoulou (1981), and Pitault et al. (1983). No evidence is found of variability. The data, together with narrow-band photometry of Torres-Dodgen & Massey (1988), have been dereddened using the interstellar extinction law of Rieke & Lebofsky (1985). The resulting energy distributions are shown in Figure 1. All of the observed near-infrared flux can easily be explained by free-free and photospheric radiation alone, with no indications of thermal emission by dust as is common among late-type WC stars (Williams, van der Hucht, & Thé 1987).

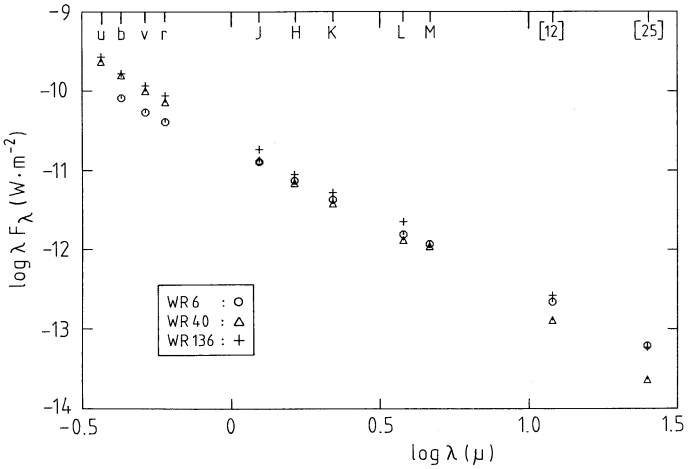

FIG. 1.—Dereddened energy distributions of the central WR stars of S308 (= HD 50896 = WR 6, van der Hucht et al. 1988), RCW 58 (HD 96548 = WR 40), and NGC 6888 (HD 192163 = WR 136), showing no dust formation in the winds of these WN stars. The spectral indices of the stars between 3.8 μm and 12 μm are −0.86, −1.04, and −0.92, respectively.

3.2. *IRAS Observations of RCW 58*

IRAS observations of RCW 58 have been made during the survey with the *IRAS* Survey Instrument at 12, 25, 60, and 100 μm, and also as additional observations with the *IRAS* Chopped Photometric Channel (CPC) at 50 μm. The *IRAS* survey data processing is described in the *IRAS* Explanatory Supplement (1988), and that of the CPC is given in the *IRAS*-DAX Chopped Photometric Channel Explanatory Supplement by Wesselius et al. (1985).

The CPC maps (version 2) have a spatial resolution of 1.′5 at 50 μm and 1.′7 at 100 μm, but the field is rather small (12′ × 9′) and the sensitivity is worse than in the survey 60 and 100 μm bands. The survey data have been examined with the Groningen Exportable Infrared High-resolution Analysis system (GEISHA; Wesselius et al. 1988). This system provides routines to make maps down to detector size resolution. It also provides an easy access to the individual detector scans over desired parts of the sky.

3.2.1. *IRAS Point Source Catalog*

The CPC map is more accurate than the *IRAS* Point Source Catalog (Version 2, 1988, hereafter PSC) as regards positions but less accurate as regards photometry. IRAS 11043−6514 [$\alpha(1950) = 11^h04^m18^s.5$, $\delta(1950) = -65°14'18''$], the WR star, has a flux 0.68 ± 0.06 Jy at 12 μm and 0.25 ± 0.04 Jy at 25 μm. The moderate quality flag at 25 μm is because the ring starts to be visible as an extended object at 25 μm and makes the background definition uncertain for the point source signal from the star.

We feel that three other sources listed in the PSC in the 25, 60, and 100 μm filters are probably bright spots in the nebula. Figure 2 shows the 50 μm CPC image; the legend identifies the location of the sources listed in the PSC. IRAS 11038−6512

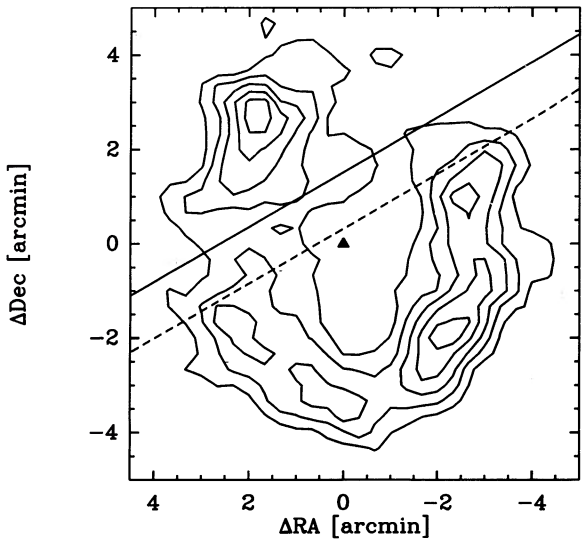

FIG. 2.—50 μm Chopped Photometric Channel (CPC) image of RCW 58, centered on WR 40. The contours are separated by 6 MJy sr^{-1} intervals. The solid line represents the 60 μm detector scan plotted in Fig. 3*a*. The dashed line represents the 100 μm detector scan plotted in Fig. 3*b*. The triangle represents the WR 40. It serves as the origin of coordinates [$\alpha(1950) = 11^h04^m18^s.5$; $\delta = -65°14'18''$]. Other sources in the PSC are IRAS 11038−6514 ($\Delta\alpha = -3.'1$, $\Delta\delta = +1.'8$), IRAS 11039−6515 ($\Delta\alpha = -2.'0$, $\Delta\delta = 1.'7$), and IRAS 11046−6512 ($\Delta\alpha = +2.'1$, $\Delta\delta = +2.'2$). Note that each of these corresponds to a peak in the brightness of the ring, and we assume that they are, in fact, nebular.

TABLE 3

FLUX DENSITIES, CORRECTED FOR COLOR, EMISSION LINES AND INTERSTELLAR EXTINCTION (Jy)

Nebula, Star	*IRAS* Band	Observation (total)	Observation (WR star)	Observation (other stars)	Nebula (including lines)	Lines (estimate)	*F*(dust)
RCW 58	12	<1.4	0.68	0.29	...	2:	0:
(WR 40)	25	8.4 ± 2.1	0.25	...	8.2	1.3	6.8
	60	43 ± 7	...	...	43	2	41
	100	22^{+20}_{-6}	...	...	22	4.4	18
S308	12	46 ± 8	1.07	40	5	6:	0:
(WR 6)	25	31 ± 5	0.62	16	15	<0.8	14
	60	161 ± 20	0.81	3	157	29	128
	100	238 ± 45	...	...	238	33	205
NGC 6888	12	7 ± 5	1.33	0.62	5	4:	0:
(WR 136)	25	76 ± 8	0.58	...	74	1	73
	60	400 ± 40	...	...	400	59	341
	100	390 ± 100	...	...	390	120	270

[$\alpha(1950) = 11^h03^m49^s.2$, $\delta(1950) = -65°12'29''$] has good quality fluxes at 12 and 60 μm. The values are 0.29 ± 0.03 and 2.1 ± 1.0 Jy, respectively. The 12 μm source is probably an unrelated field star, while the 60 μm emission is likely from the ring itself. The 60 μm point source has a signal-to-noise ratio of 11, but the correlation coefficient between the signal and the point source template is only 0.96, indicating that the source may be extended. Further support comes from the large error assigned to the 60 μm, because of different scanning angles in various *IRAS* HCONs (different parts of the extended emission observed in different scans). This point source coincides with a local maximum in the FIR emission of the ring, as seen on the CPC map.

IRAS 1103−6515 [$\alpha(1950) = 11^h03^m59^s.4$, $\delta(1950) = -65°15'58''$], with a flux of 0.54 ± 0.09 Jy at 25 μm and 5.2 ± 2.0 Jy at 60 μm, coincides with another local FIR emission maximum on the ring. The flux quality flag and the large errors indicate again that this source is part of an extended structure.

IRAS 11046−6512 [$\alpha(1950) = 11^h04^m38^s.2$, $\delta(1950) = -65°12'06''$] has a good quality flux 5.47 ± 0.60 Jy at 60 μm. This source again coincides with an local maximum of the FIR emission from the ring.

The adopted fluxes for the WR stellar and field star contributions are summarized in Table 3.

3.2.2. *IRAS Small Scale Structure Catalog*

IRAS X1104−652 [$\alpha(1950) = 11^h04^m17^s.4$, $\delta(1950) = -65°14'26''$] has good quality fluxes 11 and 41 Jy at 25 and 60 μm, respectively (*IRAS* Small Scale Structure Catalog 1988, hereafter ISSSC). The positional separation of the sources in different bands is 1'.4 in RA only. Both bands are flagged that the extended source may actually consist of two point sources merged together. This is consistent with the fact that a scan sees a narrow ring as two point sources separated by the ring diameter.

3.2.3. *CPC Maps*

The maps are suitable for a morphological study of the ring, while deriving accurate fluxes is difficult due to the small size of the maps with respect to the source diameter. The ring-shaped nebula has at 50 μm the same angular size (an outer diameter of 10'.0) and shape as the Hα image (Chu 1982), while the projected flux distribution peaks in a ring with a diameter of 5'.4.

3.2.4. *GEISHA Work*

The survey scans were calibrated with the standard method based on flashes at the beginning and end of each scan. The data in each of the four bands were co-added into a $2° \times 2°$ map with 15'' pixels. The source area was defined at 60 μm, which is the most favorable *IRAS* band for detecting ring nebulae (VBM88). The same area was then used in other bands for flux or upper limit derivations. The background was estimated by a linear fit to the immediate surrounding of the source. The error estimation is based on the uncertainty in defining the background; the low galactic latitude implies large fluctuations throughout the map area arising from unrelated objects in the line of sight. Figure 3, showing the scans at 60 and 100 μm along the cuts shown in Figure 2, illustrates the difficulties of establishing a background at 100 μm.

We find the following: (1) at 12 μm only the point sources from the *IRAS* PSC (corresponding to WR 40 and the field star) are visible on the map. The total flux is less than 1.4 Jy, which is consistent with the total flux of 1.0 Jy in the two point sources. (2) At 25 μm the ring is clearly visible as an extended source. The total flux is 8.4 ± 2.1 Jy, of which about 0.2 Jy originates from the central star. This total flux compares well with the 11 Jy in the ISSSC. (3) At 60 μm the total flux of the extended source is 42.9 ± 7.0 Jy, which compares well with the 41 Jy in the ISSSC. We assign all of the flux to the nebula since the 60 μm point sources appear as extended structures on the 50 μm CPC image (Fig. 2). From a 50 μm CPC map, M91 derived a flux from which a 60 μm flux of about 45 Jy can be estimated. There should be good agreement with our signal since there is little uncertainty in defining the background flux (see Fig. 3*a*). (4) At 100 μm the total flux of the extended source is $21.9^{+19.6}_{-5.6}$ Jy. In Figure 3*b* we illustrate by means of a one-dimensional scan the problems encountered in two dimensions when removing the background from a map. The vertical lines represent the outer limits of the nebula along the cut. Four possible backgrounds are shown across the nebula, with the highest leading to the minimum nebular flux estimate of 16.3 Jy, when similar backgrounds are integrated over the entire face of the nebula. The next (our best estimate) provides an integrated nebular flux of 21.9 Jy. The third is our estimated minimum background and gives a nebular flux of 41.5 Jy. The lowest background shown would produce a nebular flux of 107 Jy, the flux derived by M91 from a CPC map of RCW 58 which suffers from a low signal-to-noise ratio.

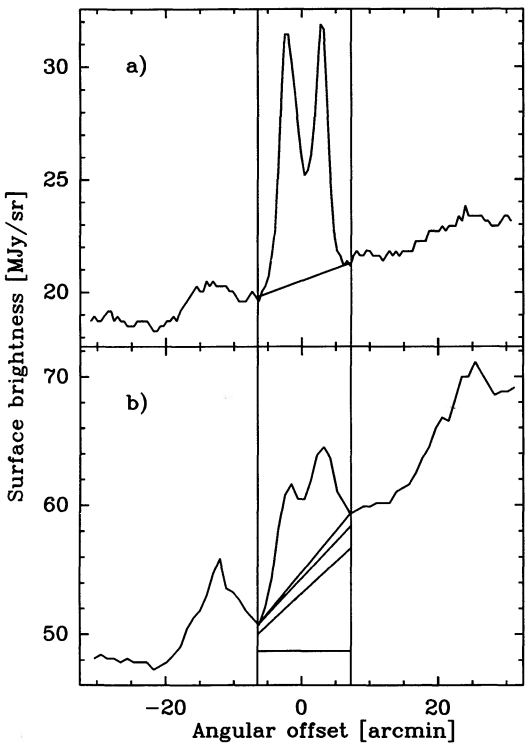

FIG. 3.—Survey detector scans over RCW 58 at (*a*) 60 μm and (*b*) 100 μm, centered on HD 96548. The directions of the cuts are shown in Fig. 2, but note the cross-scan resolution of 5′ perpendicular to the directions of the cuts. The vertical lines delineate the object. The baselines are presented within the source area. For 100 μm, the four baselines are the lower limit, the best, and the upper limit estimates, while the lowest horizontal line represents the baseline required to match the total flux estimate of Marston (1991).

3.3. *IRAS Observations of S308*

The maps from the survey scans were produced as for RCW 58 (see § 3.2.4). We find the following: (1) the 12 μm image does not reveal the ring structure, but in the defined area there is a total flux of 46 $\pm$ 8 Jy. The point source contribution from IRAS 06520−2407 (σ^1 CMa = BS 2580 = SAO 172542) is 39.10 $\pm$ 2.35 Jy, in good agreement with the aperture photometry of Hackwell & Gehrz (1974). The sum of IRAS 06516−2336, IRAS 06521−2351 (HD 50896) and 06532−2334 (WX CMa) is 2.37 $\pm$ 0.15 Jy, which leaves 5 $\pm$ 8 Jy for the nebular contribution. VBM88 obtained a nebular flux of 5.5 Jy. Since such a large correction for stellar fluxes is needed, we do not consider the 12 μm nebular flux to be usefully determined. (2) The 25 μm image has a total flux of 31 $\pm$ 5 Jy, from which 15.24 $\pm$ 0.91 Jy is from IRAS 06520−2407, 0.62 $\pm$ 0.06 Jy from IRAS 06521−2351 and 0.50 $\pm$ 0.05 Jy from IRAS 06532−2334, leaving 15 $\pm$ 5 Jy for the nebular contribution. VBM88 obtained 13 Jy. (3) The nebular 60 μm image has a total flux of 157 Jy after correcting for minor contributions from IRAS 06521−2351 (3.45 $\pm$ 0.34 Jy) and IRAS 06520−2407 (0.81 $\pm$ 0.08 Jy). There are several other 60 μm point sources in the field, but they cannot be associated with any stellar kind of object. They are, presumably, clumps in the nebula, and we feel justified in including their rather small contribution with the nebular flux. VBM88 estimated 116 Jy, after we correct for a factor of 10 typographical error in the flux listed in their Table 1 (based upon the temperature listed in their Table 1 and the 100 μm flux). (4) The total 100 μm flux is 238 $\pm$ 45 Jy, in reasonable agreement with 190 Jy in VBM88. None of the stellar objects have flux in the PSC, and we attribute all of the flux to the nebula.

3.4. *IRAS Observations of NGC 6888*

The maps from the survey scans were produced as for RCW 58. We find the following: (1) of the total 12 μm flux of 7 $\pm$ 5 Jy we subtract 1.95 $\pm$ 0.09 Jy for the PSC sources IRAS 20102+3812 (HD 192163) and IRAS 20113+3822, leaving 5 $\pm$ 5 Jy for the nebula. VBM88 and MM88 obtained 13 and 14 Jy, respectively, for the nebula plus the stars. (2) These point sources contribute only 0.96 $\pm$ 0.10 Jy at 25 μm, leaving 75 $\pm$ 8 Jy for the nebula, compared with 78 and 95 Jy for VBM88 and MM88, respectively. (3) At 60 μm, the ISSSC source IRAS X2011+380 (flux = 64 Jy) is confused with the nebula, but we do not believe it to be related. Accordingly, we assign 400 $\pm$ 40 Jy to the nebula, compared to 314 and 455 Jy assigned to it by VBM88 and MM88, respectively. These differences are easily understandable in view of the complexity of the field (see Fig. 5*c* of MM88). (4) At 100 μm, IRAS X2011+380 is so badly confused with NGC 6888 that there is no catalog flux listed. We estimate from the map that the flux of IRAS X2011+380 is 160 $\pm$ 40 Jy, leaving 390 $\pm$ 100 Jy for the nebula. VBM88 and MM88 obtained 170 and 439 Jy, respectively.

Figure 4 shows the *IRAS* survey scans at 60 and 100 μm for NGC 6888 and S308, along cuts through their central WR stars.

4. CORRECTION FOR THE ATOMIC EMISSION LINES

We have corrected for the contribution of atomic emission lines in the *IRAS* filters by estimating the fluxes of various lines and weighting them by the filter response functions at the corresponding wavelengths. The flux of each line is obtained from combining the flux of hydrogen recombination radiation (either lines or radio continuum) with the abundance of the ion producing the line relative to H (from direct observation, if possible). In some cases, where the ionic abundance is not directly observed, we must use the abundance of the element relative to H and estimate the fraction of the element in the relevant stage of ionization. The atomic constants used to predict line strengths from ionic abundances are taken from Mendoza (1983). Standard expressions for ionic emissivities

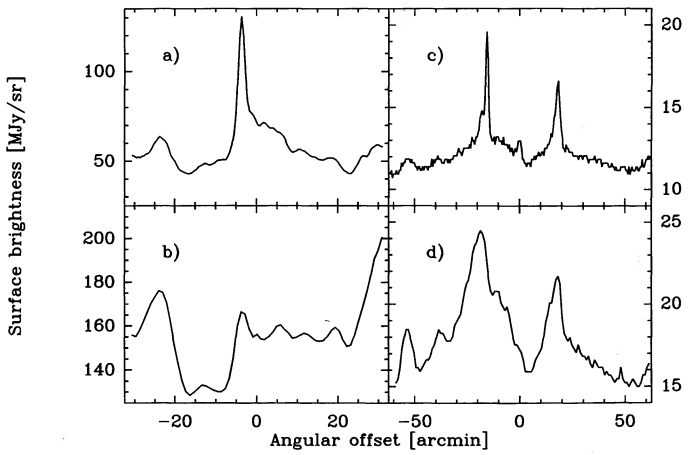

FIG. 4.—Survey detector scans over NGC 6888 at (*a*) 60 μm and (*b*) 100 μm, and S308 at (*c*) 60 μm and (*d*) 100 μm. The cuts are centered upon the central WR stars HD 192163 and HD 50896, respectively.

determine the estimated fluxes in the infrared fine-structure lines. The contributions of H and He recombinations, either lines or continuum, is negligible within the *IRAS* filter bands.

For RCW 58 we assumed that the intensity of Hβ is proportional to the *IRAS* CPC 50 μm flux (i.e., that the Hβ and 50 μm emissions are similar), and that the reddening of Hβ is constant over the face of the nebula. We determined the integral of the 50 μm map over solid angle in terms of the peak 50 μm intensity. We then used the dereddened Hβ observations of M. Rosa (1991, private communication) in three separate bright portions of the bubble to estimate the peak Hβ intensities, and from the integral we estimate the dereddened flux of Hβ. Rosa found for all three positions that $I(\mathrm{H}\beta) = (3 \pm 1) \times 10^{-15}$ ergs cm^{-2} s^{-1} arcsec^{-2}, and that the extinction (from the Balmer decrement) corresponds to $A(\mathrm{H}\beta) = 2$ mag. After correction for extinction, $F(\mathrm{H}\beta) \approx (3\text{–}6) \times 10^{-10}$ ergs cm^{-2} s^{-1}. The hydrogen recombination flux of NGC 6888 was taken from Wendker et al. (1975) at 11 cm. The $F(\mathrm{H}\beta)$ of S308 was estimated from the area of the bubble ($\approx 3.5 \times 10^6$ arcsec^2), $I(\mathrm{H}\beta) \approx (1\text{–}2) \times 10^{-16}$ ergs cm^{-2} arcsec^{-2}, and the extinction at Hβ of 1 mag (the last two quantities from M. Rosa 1991, private communication). The resulting flux is $F(\mathrm{H}\beta) \approx 1 \times 10^{-9}$ ergs cm^{-2} s^{-1}, with an uncertainty of perhaps a factor of 2. The optical line strengths were taken from Kwitter (1984) and Rosa & Mathis (1991) for RCW 58 and S308, and Kwitter (1981) for NGC 6888. The nebular temperatures used to determine ionic abundances from the optical lines were $T_e = 8000$ K and 14,000 K for RCW 58 and S308, respectively (Rosa & Mathis 1991), and 7500 K for NGC 6888 (Kwitter 1981).

The [Ne II] 12.8 μm strength follows from the rule determined empirically by Peimbert & Torres-Peimbert (1977), and confirmed by models of H II regions (Stasinska 1980; Mathis & Rosa 1991): that $(\mathrm{Ne}^+/\mathrm{Ne}^{+2}) \approx (\mathrm{O}^+/\mathrm{O}^{+2})$, which can be determined from optical lines ratios. Similarly, [N III] 57.3 μm follows from the assumption $(\mathrm{N}^+/\mathrm{N}^{+2}) \approx (\mathrm{O}^+/\mathrm{O}^{+2})$. The [S IV] 10.5 μm line is estimated from the $(\mathrm{S}^{+3}/\mathrm{S}^{+2})$ relationship with $(\mathrm{O}^+/\mathrm{O}^{+2})$ and $(\mathrm{S}^+/\mathrm{S}^{+2})$, as described in Mathis & Rosa (1991), based on models of H II regions. For Ar^{+2} there are no optical observations that are useful in determining the ionic abundance. We used the solar (Ar/O), dex(−2.2), and assumed that all Ar is in the stage Ar^{+2}. This procedure might lead to an underestimate of the strength of the [Ar III] lines because some of the bubble material has been processed by the WR star in which H-burning converted O to N without affecting Ar. Indeed, in NGC 6888 our estimate of the [Ar III] 9.0 μm plus [S IV] 10.5 μm lines is weaker by a factor of 5 than the very broad line observed in the *IRAS* LRS spectrum (VBM88), attributed by VBM88 to [Ar III] alone. We suspect that most of the 12 μm filter flux in NGC 6888 might be contributed by the [Ar III] line. However, the weakness of the 12 μm filter response sets an upper limit on the contribution of the weaker [Ar III] 21.8 μm line to the 25 μm filter, and the uncertainty in the [Ar III] 21.8 μm line cannot appreciably change our estimate of the line correction for the 25 μm filter.

We assumed that [Ar V], [Ne V], and [O IV] lines are negligible because there is no He II λ4686 observed in these bubbles, indicating that the highest stage of ionization possible is the first with an ionization potential of less than 54 eV.

The abundances of $(\mathrm{O}^{+2}/\mathrm{H}^+)$ and $(\mathrm{Ne}^{+2}/\mathrm{H}^+)$ as determined from optical spectra are almost unaffected by de-exciting collisions of ions with electrons. However, the nebular emissivity of [O III] 88 μm is reduced to 0.4 of its low-density value if $n_e \approx$ 400 cm^{-3}, as assumed by M91 and given by Kwitter (1981). We used the low-density emissivity as a conservative estimate of the line strength and therefore corrected the 88 μm flux from NGC 6888 more than did M91. For RCW 58 we used the spectrophotometry of Rosa & Mathis (1991) in place of Smith et al. (1988).

Our assumptions lead to the line strengths listed in Table 4. Many of our line strength estimates are rather uncertain, but the final result—that the lines are not major contributors to the *IRAS* filter responses—seems sound, and is in agreement with M91.

The LRS spectrum of NGC 6888 (VBM88) shows a continuous flux at 25 μm which seems in good agreement, within the considerable uncertainties of measurement, with the 25 μm filter response we attribute to the dust continuum. We estimate that if the continuum at 25 μm were flat it would correspond to about 50 Jy in the 25 μm filter. We estimate 73 Jy with our line correction. From the $F(25)/F(60)$ it is clear that there is a steep rise to longer wavelengths, and the filter response beyond 25 μm probably accounts for much of the difference.

5. DUST IN THE WR BUBBLE NEBULAE

Table 3 gives the *IRAS* fluxes, the stellar and line corrections, and the fluxes that are considered to arise from thermal emission from grains. In this section we discuss fitting the thermal emission observations with models of the dust. We begin by considering standard models of interstellar grains to explain the observed colors. However, the destruction of grains by the stellar winds might have had significant effects on the grain distributions, and we later consider modified size distributions.

In the usual interstellar medium (ISM) much of the radiation in the 12 μm *IRAS* filter is produced by processes associated with the well-known unidentified infrared bands (UIBs) observed in the wavelength range 3–13 μm (see reviews in Puget & Léger 1989; Allamandola & Tielens 1989). These bands and associated continuum typically account for about 30% of the total FIR emission. We will calculate the emission in the 25, 60, and 100 μm *IRAS* filters using the bulk optical constants of graphite and silicates. Our modeling the emission by neglecting the UIB emission processes is justified by two lines of reasoning:

1. In the diffuse ISM, the $I(12)/I(25)$ is more constant than

TABLE 4

CALCULATED EMISSION LINE CONTRIBUTIONS TO *IRAS* FLUX DENSITIES

IRAS Band (μm)	Ion	λ (μm)	Filter Trans.	RCW 58 F_λ (Jy)	S308 F_λ (Jy)	NGC 6888 F_λ (Jy)
12	Ar III	9.0	0.74	0.16	0.48	0.71:
	S IV	10.5	0.90	0.	5.9	<2.6
	Ne II	12.8	0.91	2:	0.05	2.8
	Total			3:	6.0	6
25	S III	18.7	0.54	1.3	0.73	0.85
	Ar III	21.8	0.88	0.04	0.12	0.2:
	Total			1.3	0.85	1
60	S III	33.7	0.04	0.3	0.17	0.23
	Ne III	36.1	0.07	0.04	0.04	0.12
	O III	51.7	0.67	1.5	11	29.
	N III	57.3	0.83	0.6	18.	30.
	Total			2.4	29.	59.
100	O III	88.2	0.62	4.4	33.	120.

any other color ratio, at a value of 0.5–1 in nearby molecular clouds under a variety of radiation fields and densities (Boulanger et al. 1990, and references therein). Our WR bubbles are much weaker at 12 μm, relative to 25 μm, than the nearby molecular clouds (see Table 3). Atomic emission lines can contribute all of the observed 12 μm emission for all three nebulae. Since the constancy of the $F(12)/F(25)$ ratio in the diffuse ISM is probably caused by emission for small grains/molecules, the weakness of the 12 μm signal in our WR bubbles suggests that these particles have been depleted in the dust in these bubbles.

2. Our models will suggest that the dust in at least the inner parts of the S308 and NGC 6888 bubbles has been processed enough to alter its size distribution drastically. Even the outer dust has probably been disturbed significantly because of the high radiation field to which it has been subjected. The strong variability of the $F(25)/F(100)$ and $F(60)/F(100)$ ratios in the diffuse ISM (Boulanger et al. 1990) suggests that the abundance of the small particles producing the UIBs is highly variable even within the comparatively benign conditions found in the ordinary ISM. It seems plausible that these particles would be greatly reduced in importance in the modified dust within WR bubbles because of the much higher radiation density.

For these reasons we will neglect the very small grains (say, radii of less than 10 Å) which might produce the UIBs within WR bubbles. For grains larger than this size, there are enough low-lying modes of excitation (responsible for producing the long wavelengths) so that we can safely analyze the *IRAS* intensity ratios by using bulk optical constants to calculate the thermal emission.

5.1. *The MRN/Draine-Lee Grain Model*

We will first see if the grains now in the bubbles can be interstellar grains originally in the ISM that have been displaced by the stellar winds while preserving their size distribution and composition in the process. We assume that interstellar grains are represented by the "MRN" grain mixture, derived of diffuse interstellar matter by Mathis, Rumpl, & Nordsieck (1977, hereafter MRN) and extended in wavelength (with improved optical constants) by Draine & Lee (1984). It consists of two grain types, graphites and silicates, with sizes we assume in the range $0.005\ \mu\text{m} \le a \le 0.25\ \mu\text{m}$ with a distribution $n(a)da = Ca^{-3.5}\,da$. All of the silicon is assumed to be contained in the silicates, and most of the carbon is in the graphite grains. The grains are warmed by radiation of energy density, U_ν, where

$$U_\nu = (4\pi/c)J_\nu = (4\pi/c)WF_{\nu *}\,. \tag{5.1}$$

Here W is the geometrical dilution factor ($= R_*^2/4r^2$) and $F_{\nu *}$ is the astrophysical stellar flux, which for RCW 58 we assume is the Planck function from a star at a temperature of 32,000 K. With the parameters for RCW 58 in Table 1, the frequency-integrated energy density at the mean radius in the bubble is $U = 44$ eV cm^{-3}, in contrast to $U = 0.75$ eV cm^{-3} for the galactic background radiation field (Mathis, Mezger, & Panagia 1983). The value of U in the inner part of the nebula is about 100 eV cm^{-3} at a angular radius of 2.'4, but we give special attention to the mean value of $U = 44$ eV cm^{-3}.

We will calculate the emissivities of various grain mixtures. A given grain's temperature fluctuates randomly, increasing after the absorption of a single photon and cooling until the next absorption. These fluctuations are only important for small grains ($a < 0.008\ \mu$m) because larger ones have heat capacities so large that they are not heated strongly by single photons, and they take so long to cool that they do not change their temperature appreciably between photon absorptions. Appendix A describes our calculation of the emissivities of fluctuating grains by the method of Guhathakurta & Draine (1989) and gives some results as well. For large grains whose temperatures do not fluctuate appreciably, we can use standard thermal equilibrium calculations in which the absorption and emission of energy are balanced.

Folding the calculated grain emissivities with the *IRAS* band response functions gives the theoretical *IRAS* filter fluxes. We define $\text{R25} \equiv F(25)/F(60)$ and $\text{R60} \equiv F(60)/F(100)$, where the nebular fluxes are assumed to have the line emission removed. Figure 5 compares the theoretical and observed flux ratios on a R25 versus R60 plot (which we refer to as the color-color plot). On it are shown the observed locations of the three WR ring nebulae. The heavy solid lines are labeled with the types of grains they represent. On each solid curve, the uppermost point corresponds to $U = 100$ eV cm^{-3}, the open square to $U = 44$ eV cm^{-3} (the preferred value for RCW 58), and the lowest is marked. If the lowest is $U = 3$ eV cm^{-3}, there is also a dot marking $U = 10$ eV cm^{-3}.

From Figure 5 we see that the observation of RCW 58 can be fitted, to within the very large uncertainties, by an MRN mixture, but a radiation density of $U \approx 100$ eV cm^{-3} is required. For a star with a temperature of 32,000 K, this value is reached at an angular distance of only 2.'1 from the star and is over twice the preferred energy density. This energy density (at a given angle from the star) is independent of the assumed distance, D, to the system, since the stellar luminosity, L_*, increases as the observed flux times $4\pi D^2$, and the energy density at given angle, ϕ, is given by $U = L_*/4\pi c(\phi D)^2$. However, if the stellar temperature is 42,000 K instead of our assumed value of 32,000 K (Nussbaumer et al. 1982), then $U \approx 100$ eV is plausible. This scenario would require increasing the assumed $E(B-V)$ by about 0.13 mag, which is entirely possible. However, we will discuss RCW 58 with the assumption that the Nussbaumer et al. (1982) temperature is correct.

The observations of RCW 58 could also be accommodated with an MRN mixture if the UV opacity of the grains were larger than we assumed by a factor of (100/44) = 2.2. In this case, each grain would absorb as much from the $U = 44$ eV cm^{-3} radiation field as we predict it does from the $U = 100$ eV cm^{-3}. There is considerable uncertainty in the far-infrared opacities of grains, so this possibility is not excluded, but we do not consider it likely.

There is no way of accommodating the observations of S308 and NGC 6888 with the MRN model or any single size distribution and value of U. One needs a substantial contribution to the 25 μm flux from transiently heated small grains, just as Draine & Anderson (1985) found for the typical *IRAS* observations of clouds illuminated by the interstellar radiation field, but also larger grains at a lower radiation density to explain the relatively low $F(60)/F(100)$ ratio.

5.2. *Small and Large-Grain Models*

There are unknown effects of WR wind shocks on the grain size distribution as the shocks sweep past the original interstellar grains. In this section we discuss some models of dust distributions which are plausible but which have rather arbitrary assumptions regarding the size distributions.

We continue to assume that graphite grains have 87% of the volume of the silicates, as in the MRN mixture (Draine & Lee

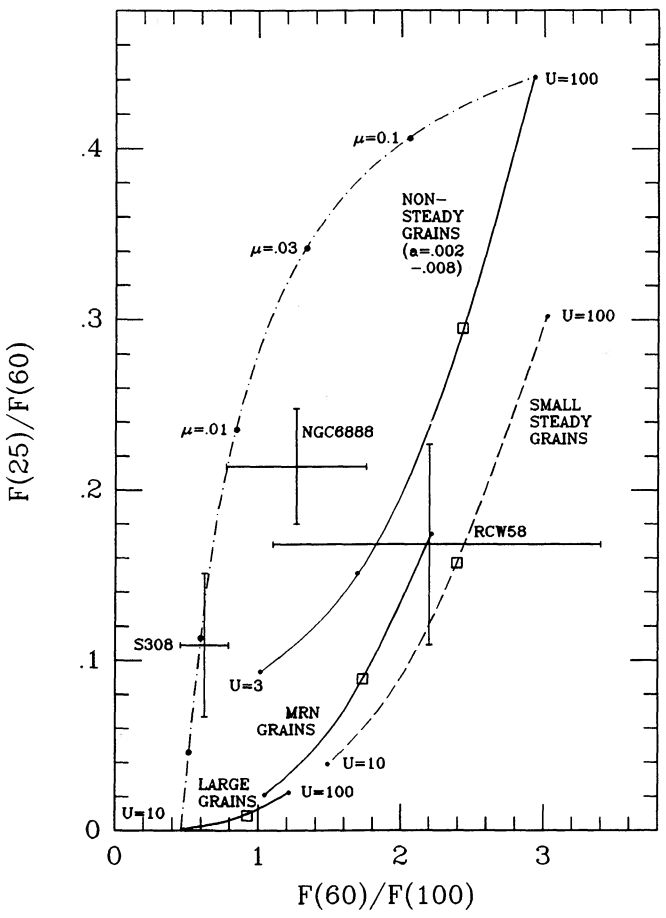

FIG. 5.—Plot of *IRAS* flux ratio $F(25)/F(60)$ (≡ R25), corrected for line emission, vs. the *IRAS* flux ratio $F(60)/F(100)$ (≡ R60). The observations of three Wolf-Rayet ring nebulae are identified. *Solid curves*: theoretical emissivities, labeled with grain types. The energy density of radiation, U, is the parameter varying along each curve, with values marked. The unmarked dot on the nonsteady grain curve is $U = 10$ eV cm^{-3}. Squares are $U = 44$ eV cm^{-3}, our preferred value for RCW 58. MRN grains = Mathis et al. (1977), as modified by Draine & Lee (1984), with 0.005 μm $\leq a \leq$ 0.25 μm and a power-law size distribution, $n(a) \propto a^{-3.5}$. Nonsteady grains = grains with the power-law, assuming a(min) = 0.002 μm, a(max) = 0.008 μm, in which the grains are transiently heated by absorption of single photon. *Dashed curve*: the same size distribution as the nonsteady-temperature grains, but with the temperature fluctuations artificially suppressed. *Solid curve near base*: the power-law size distribution but with a(min) = 0.20 and a(max) = 0.25 μm. Some values of U are identified. *Dot-dashed curve*: the locus of a combination of nonsteady-temperature grains, $U = 100$ eV cm^{-3}, with large grains, $U = 10$ eV cm^{-3}, with μ (the ratio of the mass of the small grains relative to the large) marked. The two lowest dots on the dot-dashed curve are $\mu = 0.003$ and $\mu = 0.001$. The end of the dot-dashed curve is $\mu = 0$.

1984). If there has been severe modification of the grain size distribution by the WR winds, one of the grain materials might well be depleted relative to the others, but it is beyond the scope of this paper to consider the various possibilities of grain destruction and shattering. We will assume that some dust consists of small, transiently heated grains near the exciting star, exposed to the full stellar radiation field, including the H-ionizing radiation. The small grains seem plausible because of possible effects of the Wolf-Rayet wind upon the original interstellar grains surrounding the star. For S308, NGC 6888, and one model of RCW 58 we assume that these small grains are combined with standard MRN grains farther from the star. These grains, unmodified in size distribution from the diffuse interstellar medium, are assumed to lie outside of the Strömgren sphere of the Wolf-Rayet star, so that the incident stellar flux is taken to be zero for wavelengths below the Lyman limit (912 Å) because of the absorption by nebular hydrogen. For RCW 58 we can avoid having small grains if we accept the required high radiation density. We have also constructed another model for RCW 58, referred to as RCW 58 II, in which there are small grains near the star and larger ones, farther out, smaller in size (0.005 $\leq a \leq$ 0.05 μm) than MRN.

The parameters determining the grain emissivities are T_*, U (or W), a(min), and a(max). For each of the nebulae S308 and NGC 6888 we specify beforehand the set [a(min), a(max), T_*] for both the small and large grains. The W for the inner nonsteady-temperature grains is estimated from the angular size of the 25 μm *IRAS* image, leaving W(Large) to be determined by the fit to the observed points on the color-color plot. Figures 6 and 7 show R25 and R60, respectively, for MRN grains and for various values of log (W). For MRN grains there is almost no nonsteady-temperature emission for 60 and 100 μm, and rather little for 25 μm.

The solid curve marked "Nonsteady Grains" in Figure 5 shows the emissivity for a size distribution of 0.002 μm $\leq a \leq$ 0.008 μm, a size distribution $n(a) \propto a^{-3.5}$, with the grains transiently heated by individual photon absorptions. It is not strongly affected by the value of T_*, so it is appropriate for all three nebulae. The nonsteady-temperature emission increases R25 considerably while making a much smaller change in the R60 ratio.

The solid line shown near the bottom of Figure 5 and marked "large grains" shows the results for an $a^{-3.5}$ power-law size distribution but with grains only in the size range 0.20–0.25 μm (instead of 0.005–0.25 μm in the standard MRN model). These large grains have almost no 25 μm emission but can provide reasonable amounts of 60 and 100 μm radiation.

The dot-dashed line in Figure 5 shows the results of combining various proportions of small nonsteady-temperature grains (with $U = 100$ eV cm^{-3}) with large grains located farther out in the nebula, at a point with $U = 10$ eV cm^{-3}. We define μ as the mass of small grains relative to large. The dot-dashed curve is the locus of varying μ, with values of μ marked along the curve. The upper end of the dot-dashed curve corresponds to pure small-particle emission ($\mu = \infty$), and so joins the solid line showing the emission of small particles for various values of U. The dot-dashed curve ends at $\mu = 0$, corresponding to emission from the large grains alone. Curves similar to the dot-dashed one could originate any value of U on the nonsteady-temperature grain emission curve, curve downward and to the left, and end on a large-particle (MRN or otherwise) curve. Each such curve would represent mixtures of small particles of the value of U(small) with the cold, large particles. We see that the region of the color-color plot occupied by the nebulae can be covered by these combination models.

Many models of dust emission have assumed that the temperature of each grain is steady in time. The dashed line in Figure 5 shows the colors of a mixture of small grains with the same size distribution as the nonsteady temperature grains but with the temperature fluctuations artificially suppressed. The nonsteady temperature leads to a much larger value of R25 than the artificially steady-temperature model, but has almost the same R60. Our studies of temperature fluctuations in MRN grains show that the assumption of a steady temperature for them is an excellent approximation as regards the 100 and 60 μm emissivities, and is low by 1.3 for R25.

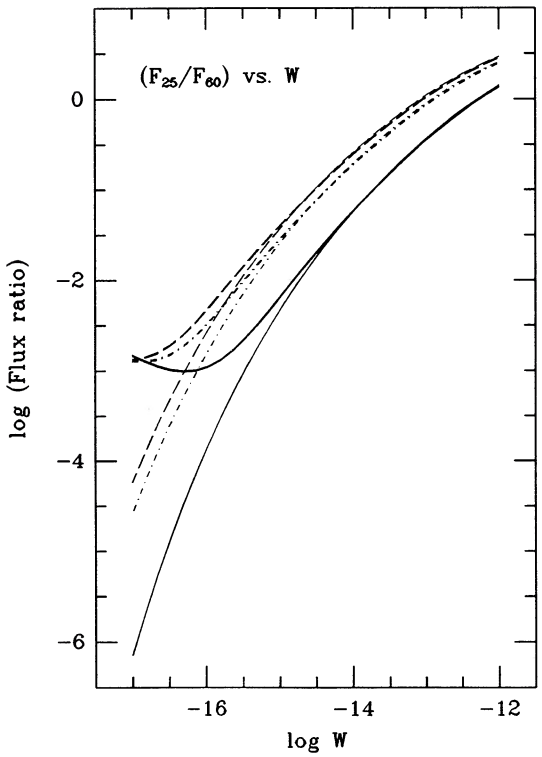

FIG. 6

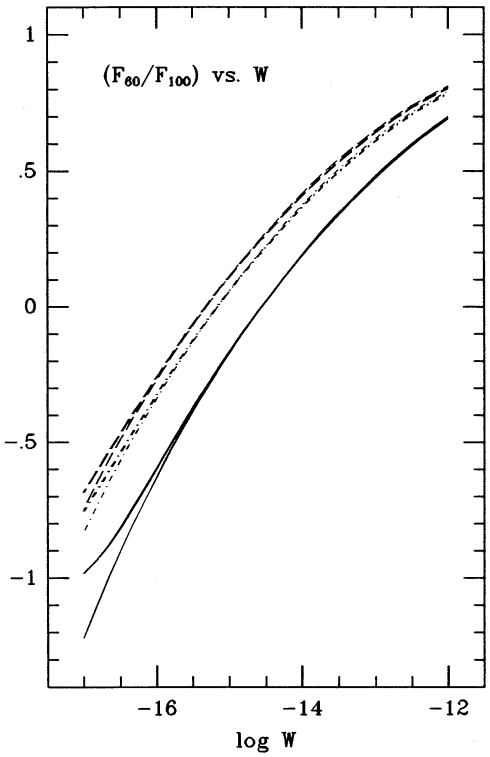

FIG. 7

FIG. 6.—Ratio of *IRAS* fluxes $F(25)/F(60)$ vs. W for MRN ($0.005 \leq a \leq 0.25$ μm) grains. The solid curves are for $T_* = 32{,}000$ K; the upper, heavier solid line is for nonsteady-temperature emission, while the lower solid curve is for the artificial assumption that each grain has a steady temperature. The dashed curves are for $T_* = 57{,}500$ K and the dot-dashed are for $T_* = 50{,}000$ K. We see that the flashing is unimportant for each value of T_* above a certain W.

FIG. 7.—Same as Fig. 6, except that R60 = $F(60)/F(100)$ is plotted instead of $F(25)/F(60)$

The solution for the dilution factor of the location of the large grains, W(large), is described in Appendix B. With that dilution factor, the mass of the dusty nebula follows from the procedure we describe next.

5.3. *Nebular Masses from Combinations of Large and Small Grains*

Figure 5 shows that in order to explain the observations of NGC 6888 and S308, and to avoid requiring too high a radiation field for RCW 58, we need to combine warm, small particles with large, cold ones at a different value of U. At frequency ν the monochromatic luminosity is given by

$$L_\nu = 4\pi(j_\nu m + J_\nu M) , \tag{5.2}$$

where j_ν is the emissivity per unit mass of the small grains, J_ν is that for the large grains, and m, M are the total masses of the small and large grains, respectively, in the nebula. We can choose different mixtures by specifying the ratios of the masses, $\mu = m/M$. The flux ratios are given by

$$\text{R25} \equiv F(25)/F(60) = [\mu j(25) + J(25)]/[\mu j(60) + J(60)] , \tag{5.3a}$$

$$\text{R60} \equiv F(60)/F(100) = [\mu j(60) + J(60)]/[\mu j(100) + J(100)] , \tag{5.3b}$$

where the band emissivities have been derived by assuming a model for the size distribution of the grains and their spatial relation to the central star (i.e., the dilution factors for the stellar radiation for both the small and large grains). The details of determining the emissivities from the assumed central star and nebular geometry are given in Appendix A. The total mass of a nebula, $(M + m)$, can be found from a fit to the observed flux in any one band, as for example:

$$L(60) = 4\pi D^2 F(60) = 4\pi M[\mu j(60) + J(60)] . \tag{5.4}$$

Any analysis of the *IRAS* emission fluxes and geometry of the nebula, coupled with assumptions about grain compositions and optical constants, can only determine the masses of the grains which are providing the radiation. There are no constraints upon the amounts of gases such as H and He that can be associated with those grains, so estimates of the total masses of the nebulae necessarily involve an assumption about the gas/dust mass ratio. For the diffuse ISM, the gas/dust ratio is strongly constrained by the observation of $A(V)/N(\text{H})$ ($= 5.3 \times 10^{-22}$ mag cm^2 atom^{-1}, Bohlin, Savage, & Drake 1978), assuming $A(V) = 3.1\ E(B-V)$. The MRN model assumed in this paper meets that extinction per H atom by placing all of the Si in $\text{Mg}_x\text{Fe}_{1-x}\text{SiO}_3$ silicates (assuming $N(\text{Si})/N(\text{H}) = 3.3 \times 10^{-6}$) and 80% of the C is in graphite. These assumptions provide a gas/dust mass ratio of 170, which may be high because we have neglected some of the Fe, Mg, besides other abundant elements which may well be in grains. On the other hand, we made a generous assumption for the undepleted abundance of C: $N(\text{C})/N(\text{H}) = 450 \times 10^{-6}$ (Meyer 1988), while several other studies (e.g., Anders & Grevesse 1989) suggest a lower C/H (360×10^{-6}), tending to make our derived gas/dust ratio low.

S308 and NGC 6888 have been modeled with nonsteady-temperature grains in the inner parts of the nebulae and the

TABLE 5

COMBINATION MODELS: MRN GRAINS PLUS SMALL GRAINS

Quantity	RCW 58 I	RCW 58 II	NGC 6888	S308 I	S308 II
Small Grains					
T_* (K)	32000[a]	32000[a]	50000[a]	57500[a]	57500[a]
a(min), a(max), (μm)	...	0.002, 0.008	0.002, 0.008	0.002, 0.008	0.001, 0.005
W (dilution factor)	...	2.02E–14	0.288E–14	0.957E–16	0.957E–16
U (eV cm^{-3})	...	100	84.9	4.94	4.94
ϕ	...	2'.4	3'	10'	10'
R25 = $F(25)/F(60)$	...	0.442	0.512	0.167	0.401
R60 = $F(60)/F(100)$	...	2.93	3.08	1.62	1.93
$j_\nu(\lambda = 60\ \mu m)$[b]	...	4.00E–11	4.58E–11	4.70E–12	3.31E–12
Large Grains (MRN: 0.005 μm < a < 0.25 μm)					
a(min), a(max) (μm)	MRN	0.005–0.05	MRN	MRN	MRN
W	2.69E–14	9.81E–15	5.25E–16	2.23E–17	7.93E–17
U (eV cm^{-3})	100	48.6	7.13	0.443	1.58
ϕ	2'.08	3'.45	6'.56	21'.44	11'.37
R25 = $F(25)/F(60)$	0.174	0.126	0.0156	0.0016	0.0037
R60 = $F(60)/F(100)$	2.21	2.12	0.907	0.293	0.502
$J_\nu(\lambda = 60\ \mu m)$[b]	2.00E–10	2.05E–11	1.65E–12	5.23E–14	2.80E–13
Combination Models					
μ[c]	0.0	0.0741	0.0239	0.0204	0.0304
$\alpha(60\ \mu m)$[c]	0.0	0.144	0.665	1.839	0.360
M(total) ($M_\odot$)[d]	0.40	0.39	20.1	136	53.5

[a] The stellar spectrum is assumed to be a complete Planck function for small grains and truncated for $\lambda < 912$ Å for MRN grains.

[b] $j_\nu(\lambda = 60\ \mu m)$ is the emissivity per gram of dust plus gas, in (ergs g^{-1} s^{-1} Hz^{-1} sr^{-1}), for small grains; J_ν is the same quantity for MRN grains, assuming the (gas + dust)/dust mass ratio is 170. For other values of this ratio, multiply by (ratio/170).

[c] μ = Mass(small grains)/Mass (MRN grains); $\alpha(60\ \mu m) = j(60\ \mu m)/J(60\ \mu m)$.

[d] M(total) = total nebular mass = mass of stellar ejecta plus swept-up interstellar material.

MRN distribution in the outer parts; RCW 58 has been modeled with MRN grains only, and also with grains smaller than MRN in both the inner and outer regions. The emissivities in the 25 μm *IRAS* band and various assumptions regarding the stellar and nebular parameters are given in Table 5. The results of the modeling with a combination of small nonsteady temperature grains plus MRN grains are also given in Table 5 in the form of μ, the ratio of the mass in the small grains relative to the MRN grains, and α_{60}, the ratio of the 60 μm emissivity of the small grains relative to the large grains. The ratio of the observed monochromatic bubble intensity to the theoretical monochromatic grain emissivity (in ergs g^{-1} sr^{-1} s^{-1} Hz^{-1}) yields the total grain mass of the grains, from which the total mass of the nebula can be estimated by assuming the gas/dust mass ratio of 170 for our model. The reader can scale the derived masses to any other gas/dust ratio. We see from Table 5 that practically all of the mass is in the large grains (>95%), which produce only 55%–60% of the 60 μm emission for RCW 58 and NGC 6888. There are two size distributions for the small grains given for S308 that provide different estimates for the nebular mass and its sensitivity on the observed colors. The model with smaller sizes (0.001 μm $\leq a \leq$ 0.005 μm) gives an estimate of only 40% as much mass as the model involving larger, and therefore cooler, small grains (0.002 $\leq a \leq$ 0.008 μm). We will discuss this discrepancy below. No doubt, changing the size distribution for the model of NGC 6888 would have a corresponding effect on our estimate of the mass of its small grains. Similarly, the mass in large grains depends upon the largest size we adopted (0.25 μm, as in Draine & Lee 1984), because in the MRN model most of the mass is contained in the large grains. Perhaps another largest size is more suitable for the heavily modified dust in WR bubbles; grains larger than 0.25 μm would add appreciably to the mass but have little emission at 60 μm or shorter. We emphasize that firm estimates of the grain mass are not possible.

For RCW 58, all of the observed emission might arise from grains in one radiation fields, such as MRN grains with $U = 100$ eV cm^{-3}. In such a case, the nebular mass follows directly from the emissivity of those grains: $M = L_\nu(4\pi j_\nu)^{-1} = D^2 F_\nu / j_\nu$. This procedure gives a mass for RCW 58 of 0.40 $M_\odot$ if $U = 100$ eV cm^{-3}, and 1.52 $M_\odot$ if $U = 44$ eV cm^{-3}. With the combination model RCW 58 II we obtain a total nebular mass of 0.39 $M_\odot$, almost the same as for the MRN grains alone but not requiring the implausibly high radiation field.

We can develop some understanding of the factors that determine the estimate of the total nebular mass by an approximate analytic treatment. Assume that the emissivities of the small grains are fixed, and focus attention on the large grains. We write $J_\nu = \kappa_\nu B_\nu(T_L)$, where T_L is the mean temperature (averaged over grain sizes) of the large grains. Equations (5.3a) and (5.3b) provide two equations in the unknowns μ and T_L. Since the large grains will have a low temperature of about 30 K, their emissivity at 25 μm will be very small, and the 60 and 100 μm bands are on the Wien (short-wavelength) side of the Planck distribution. Equation (5.3b) becomes

$$\mu = \frac{\mathrm{R25}\ \kappa(60)\ B_\nu(60,\ T_L)}{j(25) - \mathrm{R25}\ j(60)}\ , \qquad (5.5)$$

and

$$T_L = \left(1 - \frac{\nu(100)}{\nu(60)}\right) \frac{h\nu(60)}{k} \left\{\ln\left[\frac{\nu(100)}{\nu(60)}\right]^3 \frac{\kappa(100)}{\kappa(60)}\, x\right\}^1 , \quad (5.6)$$

where

$$x = \frac{J(60)}{J(100)} = \frac{\mathrm{R60}\,[\mathrm{R25}\, j(60) - j(25)]}{[\mathrm{R25}\ \mathrm{R60}\, j(100) - j(25)]} . \quad (5.7)$$

The opacity ratio $\kappa(60)/\kappa(100)$ is approximately 2.8, the small grain emissivities are given in Table 5, and the R60 and R25 are determined from the observations. The total nebular mass is related to the monochromatic luminosity at the 60 μm band by (see eq. [5.4])

$$L(60) = 4\pi[\mu j(60) + J(60)](\mu + 1)^{-1} M_{\mathrm{tot}} . \quad (5.8)$$

The numerator of this expression is proportional to $\exp[-h\nu(60)/kT_L] = \exp[-(240\ \mathrm{K})/T_L]$, since both $J(60)$ and μ are proportional to $B_\nu(60, T_L)$ (see eq. [5.6]). Hence we see that small changes in T_L lead to large changes in M_{tot}. This is also the origin of the sensitivity of the total mass to the R60 ratio we shall find below.

The masses (gas and dust) and their sensitivity to small changes of the observed flux ratios can be expressed as follows:

$$\frac{M(\mathrm{NGC\ 6888})}{M_\odot} = 20\left(\frac{\mathrm{R25}}{0.214}\right)^{0.8}\left(\frac{\mathrm{R60}}{1.26}\right)^{-3.6} ; \quad (5.9a)$$

$$\frac{M(\mathrm{S308})}{M_\odot} = 136\left(\frac{\mathrm{R25}}{0.109}\right)^{3.1}\left(\frac{\mathrm{R60}}{0.624}\right)^{-4.1} ; \quad (5.9b)$$

$$\frac{M(\mathrm{S308})}{M_\odot} = 53.5\left(\frac{\mathrm{R25}}{0.109}\right)^{0.5}\left(\frac{\mathrm{R60}}{0.624}\right)^{-3.3} . \quad (5.9c)$$

Equation (5.9b) is the relation for the small grains assumed to be in the size range 0.002 μm $\leq a \leq$ 0.008 μm; equation (5.9c) assumes the range 0.001 $\leq a \leq$ 0.005 μm.

Equations (5.9) show that the nebular mass is very sensitive to the 60 μm flux, since it enters the denominator of R25 and the numerator of R60. Thus, equation (5.9a) implies that $M(\mathrm{NGC\ 6888}) \propto F(25)^{0.8}\, F(60)^{-4.4}\, F(100)^{3.6}$. These are large exponents for the rather poorly determined *IRAS* fluxes from faint nebulae, and the uncertainty in the mass is at least a factor of 3 arising from the photometric errors alone, without considering the model of the dust grains used in the fitting.

The mass is rather insensitive to the R25 ratio when the small grains are so efficient at producing the 25 μm flux that only a small amount of them is required. This condition is not met in S308 when the larger of the small-grain size ranges is assumed (eq. [5.9b]), where the small grains needed to produce the 25 μm emission also account for two-thirds of the 60 μm flux. The model then requires a low 60 μm emission from the MRN grains, resulting in estimating $U = 0.44$ eV cm^{-3}, which is lower than the ambient interstellar radiation field of 0.75 eV cm^{-3} (neglected in our models). We conclude that this model (the small grains having the size range 0.002 $\leq a \leq$ 0.008 μm), which estimates almost 3 times as much mass as when the grains are in the smaller size range, is unreasonable for S308. The derived masses are sensitive to the assumed small-grain size distribution if the small grains account for a great deal of the 60 μm flux as well as the 25 μm.

We have not explored parameter space beyond trying two size ranges, both chosen rather arbitrarily. We could have fitted RCW 58 and NGC 6888 with models with smaller nonsteady-temperature grains, or probably almost any size range which contains enough small grains to produce adequate 25 μm emission. We consider our derived masses as merely illustrative.

A common way of expressing the mass determination is though a mean grain temperature combined with the Planck function to provide the emissivity (see M91), but one can eliminate the temperature from the mass determination and determine the sensitivity of the derived mass to the observed fluxes. If the grain temperature is taken to be the 60/100 μm color temperature, one finds

$$M_{\mathrm{dust}}/M_\odot = 4.84 \times 10^{-4}\, D_{\mathrm{kpc}}^2\, F(100)^{2.5} F(60)^{-1.5} , \quad (5.10)$$

where the fluxes are in janskys. In M91 a *dust* mass of 0.39 $M_\odot$ was derived for both RCW 58, using only R60. With our adopted gas/dust ratio of 170, after correcting for the difference in adopted distance (3 kpc for M91; 2.1 kpc for us) we would enter such a mass as 35 $M_\odot$ in Table 5, as opposed to our $\approx$1 $M_\odot$. The orders-of-magnitude difference between these results mainly arises from the differences in $F(100)$ fluxes adopted by M91 and this paper: 98 and 18 Jy, respectively.

Mass determination is more difficult than simply obtaining accurate fluxes. As is well known, it is also affected by having grains at different radiation fields such as we require for S308 and NGC 6888. If we estimate the mass of NGC 6888 from the R60 ratio alone, by using our fluxes in equation (5.10), we would obtain 0.30 $M_\odot$ of dust, corresponding to 52 $M_\odot$ of gas. With the fluxes in M91 [where the $F(60)$ is equivalent to about 420 Jy when converted from in-band flux to janskys], and our distance, we would obtain about twice as much dust (0.63 $M_\odot$). With our combination model in Table 5, we obtained 25 $M_\odot$ of gas, or 0.15 $M_\odot$ of dust. These differences of factors of 2 or more in the mass estimates with a fixed assumed distance give us a feeling for the accuracy of our estimated mass.

It is easy to imagine that all of the mass we estimate for RCW 58, $\approx$1 $M_\odot$, is stellar ejecta. The masses we derive for NGC 6888 and S308 (20 and 50 $M_\odot$, respectively) are not impossibly large for having been ejected by the WR stars, but it seems very possible that most of these bubbles consists of compressed ISM. The density of the ISM is highly variable but might plausibly range from $N_{\mathrm{H}} < 0.01$ cm^{-3} in ionized parts of the diffuse ISM to values $N_{\mathrm{H}} \approx 10$ cm^{-3} or more in neutral cloud regions. With our distances and the angular sizes for these bubbles, the masses of ISM originally within the present bubble are $(43 n_{\mathrm{H}}, 260 n_{\mathrm{H}})\, M_\odot$, respectively. Thus, previous densities of $n_{\mathrm{H}} = (0.5, 0.2$ H cm$^{-3})$, respectively, are adequate to account for all of the mass we estimate in the bubbles. It is likely that densities of this order were present.

We conclude that assumptions about the geometry and size distribution of nebular grains make large differences to the derived grain masses. We have not explored parameter space to any great extent, but the differences in the masses we derive with two rather arbitrarily chosen grain size distributions show that the question of masses of grains in the WR bubbles is still rather open, except that the types of grains which produce ordinary interstellar extinction are certainly inadequate for explaining the relatively strong 25 μm fluxes in dilute radiation fields.

6. SUMMARY AND CONCLUSIONS

1. We have produced high-resolution far-infrared images of the Wof-Rayet bubble RCW 58 and estimated the *IRAS* colors

of S308 and NGC 6888. The *IRAS* fluxes of these nebulae at 25, 60, and 100 μm arise from dust emission rather than from atomic emission lines.

2. Because of the low 12 μm fluxes from the bubbles, we calculate the emission on the basis of continuum radiation from dust, rather than emission from the "unidentified infrared bands" and continuum associated with them. Presumably, the radiation and stellar wind of the WR star have destroyed most of the materials giving rise to the infrared band emissions.

The WR ring nebulae NGC 6888 and S308 lie in a region of the $F(25)/F(60) - F(60)/F(100)$ color-color plot that cannot be produced from an interstellar MRN grain mixture with size limits of 0.005–0.25 μm, because the MRN mixture has grains so large that they produce 25 μm radiation inefficiently. If the stellar radiation density is large enough to produce the proper $F(25)/F(60)$, the $F(60)/F(100)$ ratio is too large for RCW 58. A similar result applies to explaining the average colors of the diffuse interstellar medium. The emission in the *IRAS* 25 μm filter must be contributed by transient heating of small grains or emissions from molecules excited by absorption of a single photon.

Small grains alone overproduce 60 μm emission relative to 100 μm, so larger grains, possibly the type found in interstellar dust (MRN), are required. These larger grains are cooler than the nonsteady-temperature grains and so contain most of the grain mass.

RCW 58 has an uncertain $F(100\ \mu\text{m})$ flux. With our best estimate, a simple MRN grain mixture can fit both the R25 and R60 ratios, but the required radiation energy density (100 eV cm^{-3}) is higher than we would expect for the mean (44 eV cm^{-3}). Alternatively, we can fit RCW 58 with a mixture of small (0.002–0.008 μm) grains and somewhat larger (0.005–0.05 μm) farther from the star, with the radiation density we expect from the star.

3. We have been able to explain the relatively large observed 25 μm fluxes in NGC 6888 and S308 in terms of emission from small grains that are transiently heated to temperatures well above 100 K. A small amount of small grains would remove the discrepancy in radiation energy density for RCW 58 as well. It is plausible that small grains could be produced by the interaction of the stellar winds in the inner regions of the nebula, perhaps by shattering of previously larger grains. In NGC 6888 we chose to fix the grain sizes to lie between 0.002 and 0.008 μm, but the grains must be even smaller in S308 (for which we achieved a plausible, but not unique, fit with grains in the range 0.001–0.005 μm).

4. The derived mass estimates are quite sensitive to the observed fluxes. The two orders of magnitude difference in mass estimate between us and M91 for RCW 58 is mainly caused by a discrepancy of a factor of 4.9 in the inband 100 μm flux. Even if the fluxes are accurately observed, differences in models assumptions (grain sizes and placement within the bubble) can easily cause discrepancies of factors of two or more between models. We consider the numerical estimates of the masses in Table 5 as illustrative only.

5. Plots of the grain emissivities are given in Figure 9 and the colors of the emissions in Figures 6 and 7, both as functions of the dilution factor W.

We thank Michael Rosa for communicating optical spectra of S308 and RCW 58 prior to publication, Eric L. Jensen for assistance with the computations, A. P. Marston and the anonymous referee for helpful comments on the manuscript. This research has been partially supported by NASA contract 957996 through the Astrophysics Data Program and NASA grants NAGW-2210 (to J. P. C.) and NAGW-1768 (to J. S. M.). T. P. acknowledges financial support from the Academy of Finland. K. A. v. d. H. gratefully acknowledges generous hospitality at Washburn Observatory through NASA contract 957996.

APPENDIX A

THE CALCULATION OF EMISSION FROM NONSTEADY-TEMPERATURE GRAINS

Many researchers have studied the effects of temperature fluctuations in grains (Duley 1973; Draine & Anderson 1985; Dwek 1986; Guhathakurta & Draine 1989). The temperature distribution for small grains can be very broad, and grains at temperatures above the thermal equilibrium value can lead to a greatly increased 12 and 25 μm fluxes. The grains cooler than the mean can also lead to a relative increase in the 100 μm flux, as shown in Figure 5 by the fact that R60 at the uppermost points ($U = 100$ eV cm^{-3}) of the nonsteady-temperature grains is smaller than the steady-temperature value for the same small-grain size distribution. In this paper we used the formulation and heat capacities of Guhathakurta & Draine (1989) and the absorption efficiencies of Draine & Lee (1984).

Grains which are transiently heated and subsequently cool have a steady state distribution function, in which the number of grains per unit time leaving a certain temperature range equals the number entering that range. The process is similar to the statistical equilibrium of the populations of atomic levels in a stellar atmosphere. Probability distributions for several sizes of silicate grains are shown in Figure 8 for $T_* = 32{,}000$ K, $U = 44$ eV cm^{-3}. Note that there can be a wide range in temperature, especially for the smallest grains, ranging from 12 K to several times the thermal equilibrium value of about 60 K.

The emissivities of grains depend upon their size distribution and the spectrum and dilution factor of the incident radiation field. In this paper we have considered only three stellar temperatures (with and without being truncated at the Lyman limit) and two ranges of small grain sizes. It is illustrative to show how the emissivities and colors vary with the dilution factor, W. Figure 9 shows the emissivities for both MRN and small grains with sizes in the range $0.002 \leq a \leq 0.008$ μm, as were used on all three nebulae, plotted against log (W). Also shown are the emissivities for $0.001 \leq a \leq 0.005$ μm for $T_* = 57{,}500$ K. The minimum values of W shown correspond to a radiation energy density of roughly the mean interstellar value (0.75 eV) for the largest value of T_*(57,500 K) With good accuracy the reader can use these curves for other stellar temperatures by converting the desired W to radiation energy density U and doing the same for the plotted curves. We choose to use W because it is more physical for a given stellar luminosity and distance from the star.

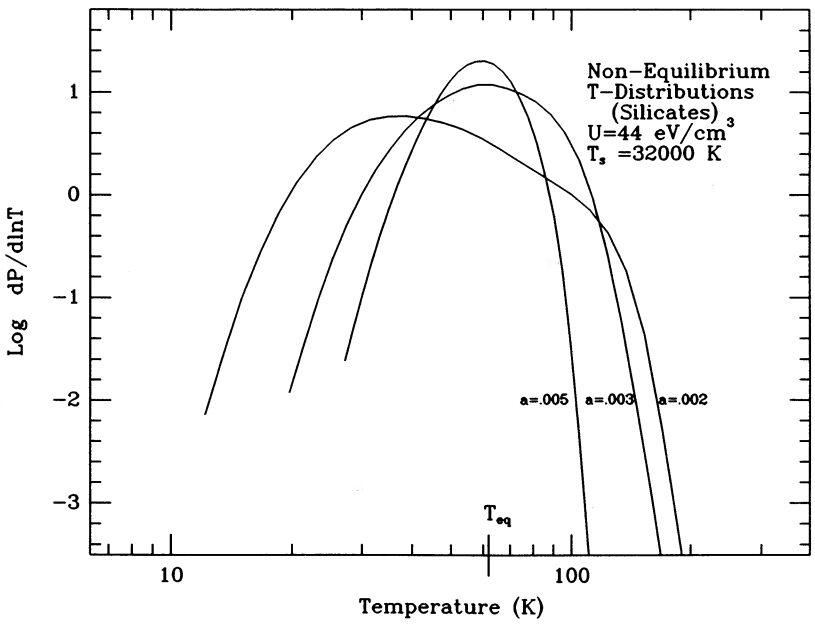

FIG. 8.—Temperature distribution functions plotted vs. temperature for silicate grains of three different grain radii as shown. The results are for a model with an incident radiation field of a dilute $T = 32{,}000$ K Planck function, at an energy density of $U = 44$ eV cm^{-3} appropriate for RCW 58.

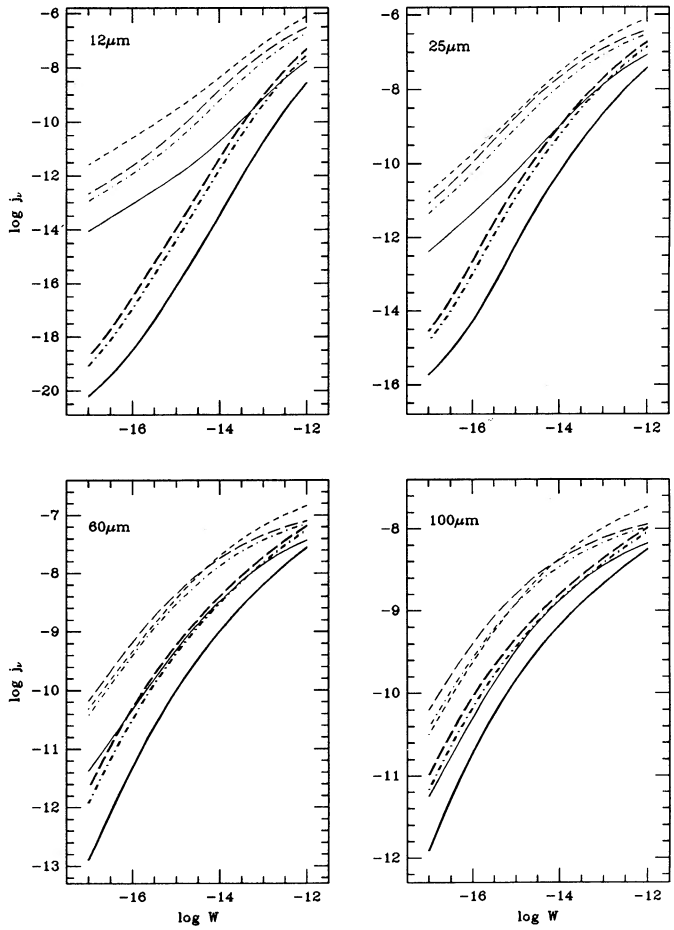

FIG. 9.—Emissivities of nonsteady-temperature grains for various size distributions and stellar temperatures plotted against the geometrical dilution factor W. *Solid curves*: $T_* = 32{,}000$ K; *dot-dashed curve*: $T_* = 50{,}000$ K; *long dashes*: $T_* = 57{,}500$ K. *Heavy curves*: the MRN size distribution, with $0.005 \leq a \leq 0.25$ μm, and the stellar flux truncated at the Lyman limit. Light curves: $0.002 \leq a \leq 0.008$ μm, except that the light short-dashed curve is for $T_* = 57{,}500$ K, $0.001 \leq a \leq 0.005$ μm. The stellar fluxes for the light curves are not truncated at the Lyman limit.

Figures 6 and 7 show the colors of the emitted radiation of the same grain mixtures and values of T_* as in Figure 9. The light lines show the commonly assumed case: that all grains have a steady temperature. The heavy lines show the effects of an nonsteady temperature distribution on the colors. One notes that at high values of W the nonsteady nature of real grain emission has no effect; the grains are large enough to hold their heat between the frequent absorptions. At low values of W, the colors of the correct (nonsteady) emission are dramatically different from those of steady-temperature models, in the sense that the 25 μm is vastly increased. There is almost no effect for the R60 ratio. Not shown in these figures is that all colors approach constant values, independent of W, for very low values of W. This situation occurs when the radiation is so dilute that every grain has time to cool to a temperature so low that it does not emit appreciably at 100 μm before absorbing another photon. Shown in Figure 6 is the next regime which arises: The 60 μm emission increases faster than the 25 μm as W is increased from very low values, because the grains are warm enough to radiate at 60 μm when they absorb a second photon.

APPENDIX B

THE ESTIMATION OF MASSES FROM THE GRAIN EMISSIVITIES

Figures 6 and 7 allow us to derive the mass of the ring nebulae $M_{\rm tot}$, and the fractions of the nebulae in small grains, m, and large grains, M, as follows:

Let R25 $\equiv F(25)/F(60)$ and R60 $\equiv F(60)/F(100)$ be the observed ratios of *IRAS* fluxes. We then have

$$\mathrm{R25} = \frac{\mu j(25) + J(25)}{\mu j(60) + J(60)}; \tag{B1}$$

$$\mathrm{R60} = \frac{\mu j(60) + J(60)}{\mu j(100) + J(100)}. \tag{B2}$$

From solving equations (B1) and (B2) for μ, and setting $J(25) = 0$ because large grains are cold, we get

$$\mu = -\frac{\mathrm{R25}\ J(60)}{[\mathrm{R25}\ j(60) - j(25)]}. \tag{B3}$$

We multiply equation (B1) by (B2) and solve for μ to get

$$\mu = -\frac{\mathrm{R25\ R60}\ J(100)}{[\mathrm{R25\ R60}\ j(100) - j(25)]}. \tag{B4}$$

Equating equations (B3) and (B4), we get ratios involving either small or large grains:

$$\frac{\mathrm{R25}\ J(60)}{\mathrm{R25\ R60}\ J(100)} = \frac{\mathrm{R25}\ j(60) - j(25)}{\mathrm{R25\ R60}\ j(100) - j(25)}, \tag{B5}$$

Dividing numerator and denominator by $J(60)$ on the left-hand side of equation (B5), and $j(60)$ on the right-hand side, we get ratios of observed quantities and ratios of emissivities:

$$\left[\frac{J(60)}{J(100)}\right] = \frac{\mathrm{R25} - [j(25)/j(60)]}{\mathrm{R25}\ [j(100)/j(60)] - [j(25)/j(60)]/\mathrm{R60}}. \tag{B6}$$

From our models we can calculate the ratios of the emissivities of each grain component (either the large grains or transiently heated small grains), so the quantities in brackets in equation (B6) are predicted by the assumed geometry and size distributions. Note that the left-hand side depends only upon the large grains and the right on observed quantities and the properties of the small grains. The required ratios of emissivities are shown in Figures 6 and 7.

Our procedure is to specify all quantities on the right-hand side of equation (B6) by giving a value for the angular radius to the inner boundary of the nebulae, $\phi_1 = r_1/D$. Then

$$W_1 = R_*^2/(4r_1^2) = R_*^2/(2\phi_1 D)^2, \tag{B7}$$

where D is the distance to the nebula, and R_* is derived from the stellar luminosity and assumed stellar temperature, T_*. With this dilution factor known, Figures 6 and 7 give (R25, R60) for a specified [a(min), a(max), T_*]. Equation B6 now provides a relation to find the dilution factor W for the large grains. We can now get the mass of the nebulae. Using equation (B3) or (B4) for μ, the ratio of the band luminosity from small grains to that in large grains (at 60 μm) is

$$\alpha = \mu j(60)/J(60),$$

and the total mass of the nebula is

$$M_{\rm tot} = \left[\frac{\mu + 1}{\alpha + 1}\frac{L_{60}}{4\pi J(60)}\right],$$

where $L(60)$ is the observed luminosity in the 60 μm band, and the masses of the large and small grain components are

$$M_{\rm large} = M_{\rm tot}/(\mu + 1); \qquad M_{\rm small} = \mu M_{\rm large}.$$

REFERENCES

Allamandola, L. J., & Tielens, A. G. G. M., eds. 1989, IAU Symp. 135, Interstellar Dust (Dordrecht: Kluwer), 530
Allen, D. A., Swings, J. P., & Harvey, P. M. 1972, A&A, 20, 333
Anders, E., & Grevesse, N. 1989, Geochim. Cosmochim. Acta, 53, 197
Bohlin, R. C., Savage, B. D., & Drake, J. F. 1978, ApJ, 224, 132
Boulanger, F., Falgarone, E., Puget, J. L., & Helou, G. 1990, ApJ, 364, 136
Chu, Y.-H. 1982, ApJ, 254, 578
———. 1988, PASP, 100, 986
———. 1991, in IAU Symp. 143, Wolf-Rayet Stars and Interactions with Other Massive Stars in Galaxies, ed. K. A. van der Hucht & B. Hidayat (Dordrecht: Kluwer), 349
Chu, Y.-H., Treffers, R. R., & Kwitter, K. B. 1983, ApJS, 53, 937
Cohen, M., Barlow, M. J., & Kuhi, L. V. 1975, A&A, 40, 291
Draine, B. T., & Anderson, N. 1985, ApJ, 292, 494
Draine, B. T., & Lee, H. M. 1984, ApJ, 285, 89
Duley, W. W. 1973, Ap&SS, 23, 43
Dwek, E. 1986, ApJ, 302, 363
Guhathakurta, P., & Draine, B. T. 1989, ApJ, 345, 230
Hackwell, J. A., & Gehrz, R. D. 1974, ApJ, 194, 49
Hackwell, J. A., Gehrz, R. D., & Smith, J. R. 1974, ApJ, 192, 383
Hamann, W.-R., Schmutz, W., & Wessolowski, U. 1988, A&A, 194, 190
IRAS Catalogs and Atlases: Explanatory Supplement, 1988, ed. Beichman, C. A., Neugebauer, G., Habing, H. J., Clegg, P. E., & Chester, T. J. (Washington, DC: GPO)
IRAS Point Source Catalog, Version 2, 1988, Joint *IRAS* Science Working Group (Washington, DC: GPO) (PSC)
IRAS Small Scale Structure Catalog, 1988, prepared by G. Helou & D. Walker (Washington, DC: GPO) (ISSSC)
Kwitter, K. B. 1981, ApJ, 245, 154
———. 1984, ApJ, 287, 840
Marston, A. P. 1991, ApJ, 366, 181 (M91)
Marston, A. P., & Meaburn, J. 1988, MNRAS, 235, 391 (MM88)
Massey, P. 1984, ApJ, 281, 789
Mathis, J. S., Mezger, P. G., & Panagia, N. 1983, A&A, 128, 212
Mathis, J. S., & Rosa, M. R. 1991, A&A, 245, 625
Mathis, J. S., Rumpl. W., & Nordsieck, K. H. 1977, ApJ, 217, 425 (MRN)
Mendoza, C. 1983, in IAU Symp. 103, Planetary Nebulae, ed. D. R. Flower (Dordrecht: Reidel), 143
Meyer, J.-P. 1988, in Origin and Distribution of the Elements, ed. G. J. Mathews (Singapore: World Scientific), 337
Nussbaumer, H., Schmutz, W., Smith, L. J., & Willis, A. J. 1982, A&AS, 47, 257
Peimbert, M., & Torres-Peimbert, S. 1977, MNRAS, 179, 217
Pitault, A., Epchtein, N., Gomez, A., & Lortet, M. C. 1983, A&A, 120, 53
Puget, J. L., & Léger, A. 1989, ARA&A, 27, 161
Rieke, G. H., & Lebofsky, M. J. 1985, ApJ, 288, 618
Rosa, M. R. 1987, in IAU Symp. No. 122, Circumstellar Matter, ed. I. Appenzeller & C. Jordan (Dordrecht: Reidel), 457
Rosa, M. R., & Mathis, J. S. 1991, A&A, in preparation
Schmutz, W., Hamann, W.-R., & Wessolowski, U. 1989, A&A, 210, 236
Smith, L. F., & Maeder, A. 1989, A&A, 211, 71
Smith, L. J., Pettini, M., Dyson, J. E., & Hartquist, T. W. 1988, MNRAS, 234, 625
Stasinska, G. 1980, A&A, 84, 320
Torres-Dodgen, A. V., & Massey, P. 1988, AJ, 96, 1076
Van Buren, D., & McCray, R. 1988, ApJ, 329, L93 (VBM88)
van der Hucht, K. A., Hidayat, B., Admiranto, A. G., Supelli, K. R., & Doom, C. 1988, A&A, 199, 217
van der Hucht, K. A., Jurriens, T. A., Olnon, F. M., Thé, P. S., Wesselius, P. R., & Williams, P. M. 1985, in Birth and Evolution of Massive Stars and Stellar Groups, ed. W. Boland & H. van Woerden (Dordrecht: Reidel), 167
Voels, S. A., Bohannan, B., Abbott, D. C., & Hummer, D. G. 1989, ApJ, 340, 1073
Wendker, H. J., Smith, L. F., Israel, F. P., Habing, H. J., & Dickel, H. R. 1975, A&A, 42, 173
Wesselius, P. R., Beintema, D. A., de Jonge, A. R. W., Jurriens, T. A., Kester, D. J. M., van Weerden, J. E., de Vries, J., & Perault, M. 1985, IRAS-DAX Chopped Photometric Channel Explanatory Supplement (Groningen: SRON-SRG)
Wesselius, P. R., Bontekoe, T. R., de Jonge, A. R. W., & Kester, D. J. M. 1988, in Astronomy from Large Databases, ESO Conference and Workshop Proceedings, 28, 85
Williams, P. M., & Antonopoulou, E. 1981, MNRAS, 196, 915
Williams, P. M., & Eenens, P. R. J. 1989, MNRAS, 240, 445
Williams, P. M., van der Hucht, K. A., & Thé, P. S. 1987, A&A, 182, 91
Willis, A. J. 1982, MNRAS, 198, 897
Willis, A. J., Howarth, I. D., Smith, L. J., Garmany, C. D., & Conti, P. S. 1989, A&AS, 77, 269